Detailed study of the decay ^{31}Cl($\beta\gamma$)^{31}S

M. B. Bennett,[1,2,3,*] C. Wrede,[1,2,†] S. N. Liddick,[2,4] D. Pérez-Loureiro,[1,2] D. W. Bardayan,[5] B. A. Brown,[1,2] A. A. Chen,[6] K. A. Chipps,[7,8] C. Fry,[1,2,3] B. E. Glassman,[1,2] C. Langer,[2,3] N. R. Larson,[2,4] E. I. McNeice,[6] Z. Meisel,[1,2,3] W. Ong,[1,2,3] P. D. O'Malley,[5] S. D. Pain,[7] C. J. Prokop,[2,4] H. Schatz,[1,2,3] S. B. Schwartz,[1,2,9] S. Suchyta,[2,4] P. Thompson,[7,8] M. Walters,[6] and X. Xu[1,2]

[1]*Department of Physics and Astronomy, Michigan State University, East Lansing, Michigan 48824, USA*
[2]*National Superconducting Cyclotron Laboratory, Michigan State University, East Lansing, Michigan 48824, USA*
[3]*Joint Institute for Nuclear Astrophysics, Michigan State University, East Lansing, Michigan 48824, USA*
[4]*Department of Chemistry, Michigan State University, East Lansing, Michigan 48824, USA*
[5]*Department of Physics, University of Notre Dame, Notre Dame, Indiana 46556, USA*
[6]*Department of Physics and Astronomy, McMaster University, Hamilton, Ontario L8S 4M1, Canada*
[7]*Oak Ridge National Laboratory, Oak Ridge, Tennessee 37831, USA*
[8]*Department of Physics and Astronomy, University of Tennessee, Knoxville, Tennessee 37996, USA*
[9]*Department of Geology and Physics, University of Southern Indiana, Evansville, Indiana 47712, USA*

(Received 28 October 2017; published 14 June 2018)

Background: ^{31}Cl is a neutron-deficient isotope with a half-life of $T_{1/2} = 190(1)$ ms. The nuclear structure of its daughter, ^{31}S, is important for the determination of the thermonuclear ^{30}P$(p,\gamma)^{31}$S reaction rate, which affects the final isotopic abundances of the ejecta from classical oxygen-neon novae.
Purpose: We aim to determine the β feedings, γ-decay branchings, and excitation energies of states populated in ^{31}S and create a comprehensive decay scheme for comparison with predictions based on the shell model.
Methods: Using a ^{31}Cl rare istope beam implanted into a plastic scintillator and an array of high-purity Ge detectors, γ rays from the ^{31}Cl$(\beta\gamma)^{31}$S decay sequence were measured. Shell-model calculations using the USDB and the recently-developed USDE interactions were performed for comparison.
Results: A ^{31}Cl β-decay scheme was constructed from the experimental data and compared to the USDB and USDE shell-model calculations based on the β feeding and γ-decay branches of each observed state. 33 new γ-ray transitions and ten new β decay branches were observed. The β feeding and γ-decay branches of each observed state were compared to those from the USDB and USDE shell-model calculations. For every allowed transition predicted by the USD calculations up to an excitation energy of 6.4 MeV in ^{31}S, an analogous transition was found in the experimental data, enabling a one-to-one comparison with the shell model. Using these identifications, spin and parity arguments were made for observed states.
Conclusions: The new ^{31}Cl γ-decay scheme presented in this work is the most complete and precise one for this nucleus constructed to date, incorporating statistics over an order of magnitude higher than previous work on ^{31}Cl β-delayed γ decay. Of particular interest is the discovery of a 6390-keV state that mixes with the isobaric analog state and affects the ^{30}P$(p,\gamma)^{31}$S reaction rate. Other states observed in the decay are not expected to strongly affect the ^{30}P$(p,\gamma)^{31}$S reaction rate, but the comprehensive comparison to the shell model helps to clarify spin and parity assignments of resonances that might affect the rate.

DOI: 10.1103/PhysRevC.97.065803

I. INTRODUCTION

The ^{31}S isotope has been a subject of nuclear structure studies for several decades because it is critical for answering several important astrophysical questions. It lies at a potential bottleneck for nova nucleosynthesis: the final $A \geqslant 30$ isotopic abundances of classical novae are determined by the rate of the ^{30}P$(p,\gamma)^{31}$S reaction. In turn, the rate of this reaction also helps determine the maximum temperature novae may reach [1], and can help answer the question of presolar grain origins [2–6].

Indeed, much work to determine the nuclear structure of ^{31}S has been motivated by the ^{30}P$(p,\gamma)^{31}$S rate in novae, which is likely governed by a number of narrow resonances in the energy region above the proton emission threshold of 6130.9(4) keV [7]. Unfortunately, because a radioactive ^{30}P beam with sufficient intensity does not exist, it is not currently possible to measure these resonances directly. Instead, various indirect techniques have been used (see Sec. II). Determining the spins and parities of these resonances is critical to determining the resonance strengths, which set the reaction rate at nova temperatures:

$$N_A\langle\sigma v\rangle \propto \sum_i \omega\gamma_i e^{-E_{r_i}/kT}. \quad (1)$$

*bennettm@nscl.msu.edu
†wrede@nscl.msu.edu

Here $N_A\langle\sigma v\rangle$ is the thermonuclear resonant reaction rate, E_r is the resonance energy, T the temperature, and the resonance strength $\omega\gamma$ is given by

$$\omega\gamma = \frac{(2J_r+1)}{(2J_t+1)(2J_p+1)}\frac{\Gamma_p\Gamma_\gamma}{\Gamma_p+\Gamma_\gamma} \quad (2)$$

where, for the ^{30}P$(p,\gamma)^{31}$S reaction, $J_{r,p,t}$ represents the spin of the ^{31}S resonance state, proton ($J = 1/2$), or ^{30}P nucleus ($J = 1$), and Γ_p and Γ_γ represent the proton and γ-ray partial widths of the resonance, respectively. Determining the spins, energies, and partial widths of the resonance states, then, sets the strength, which in turn is proportional to the reaction rate for resonant capture through that state. Parity constraints are also needed, as the positive parity of ^{30}P dictates that the $l = 0$ proton captures, which are devoid of a centrifugal barrier, will populate states which are also positive parity.

However, due in part to the nature of the experimental methods used to study the isotope, spin and parity constraints on several of these states are ambiguous, and in some cases even contradictory (see Sec. II for an more detailed discussion of ^{31}S studies). Of paramount importance in determining the ^{30}P$(p,\gamma)^{31}$S rate, then, are experimental studies with reliable constraints on the spins and parities of populated ^{31}S levels. The β decay of ^{31}Cl is useful in this regard, as allowed transitions from the $J^\pi = 3/2^+$ ^{31}Cl ground state strongly populate only $J^\pi = (1/2,3/2,5/2)^+$ states in ^{31}S according to the β-decay selection rules. ^{31}Cl can thus be used not only to obtain new information relevant to the ^{30}P$(p,\gamma)^{31}$S rate, but to reduce ambiguity in the current set of data on ^{31}S structure in the regions below and above the proton emission threshold.

In addition to the astrophysical motivations for studying ^{31}S, this sd-shell nucleus can be useful as a test of nuclear shell-model calculations that predict both γ-decay branches for excited ^{31}S states and β feeding intensities from the parent nucleus ^{31}Cl. β decay schemes derived from shell-model calculations employing, for example, the commonly used USDB interaction [8], can be compared to experimentally determined schemes to refine the accuracy of the predictions.

Study of ^{31}Cl can therefore be incredibly useful not only for constraining the ^{30}P$(p,\gamma)^{31}$S rate, but as a test of the shell model itself. In light of this fact, and the fact that previous experimental studies of ^{31}S have produced ambiguities addressed in the present study, a short discussion of previous studies relevant to the results of the present study will be presented in the following section.

II. BRIEF CONTEXT OF WORK ON ^{31}S

As discussed in Sec. I, the various experimental methods used to study ^{31}S preclude perfectly unambiguous constraints on the nuclear states relevant to ^{30}P$(p,\gamma)^{31}$S. The Gamow window for ^{30}P$(p,\gamma)^{31}$S at peak nova temperatures extends about 600 keV above the ^{31}S proton threshold, so the discovery of all resonance states in the region and the determination of their properties are of key importance for constraining the ^{30}P$(p,\gamma)^{31}$S rate. A detailed overview of the history of ^{30}P$(p,\gamma)^{31}$S studies which have been used to piece together the current understanding of the ^{31}S resonances in the energy region of interest [9–21] up to 2014 is given in Ref. [22], and several recent studies have been published as well [23–25]. The reader is referred to these works for a full history; here we will briefly discuss selected experiments which are most relevant to the present work.

Kankainen *et al.* published the first work influenced by astrophysical motivations for the study of ^{30}P$(p,\gamma)^{31}$S, a β-decay study of ^{31}Cl [12]. The experiment measured both the β-delayed proton emission and β-delayed γ decay of ^{31}S states above the proton threshold. Multiple results were obtained, including the discovery of a state then evaluated at 6921(15) keV through measurement of proton emissions, γ rays corresponding to deexcitation of the first two excited ^{31}S states, and the first definitive identification of the proton-unbound ^{31}S isobaric analog state (IAS) through measurement of its γ decay. Another study of both the β-delayed γ decay and β-delayed proton decay of ^{31}Cl, performed in 2011, improved upon the sensitivity of Ref. [12], reporting the observation of the γ decay of the ^{31}S IAS to the ground state for the first time and a number of other γ-ray transitions [13].

Also relevant to the present work are the ^{31}P$(^3$He$,t)^{31}$S reaction studies of Wrede *et al.* and Parikh *et al.* [16,17], which reported evidence for many proton-unbound ^{31}S states, including one at 6400 keV, and the ^{28}S$(\alpha,n\gamma\gamma)^{31}$S reaction studies of Doherty *et al.*, which reported a $J^\pi = 5/2^+$ resonance at 6393 keV [20,21]. The latter claimed, based on comparisons to the mirror nucleus ^{31}P, that all relevant states in the energy region had been identified, implying that the state observed in Refs. [16,17] was identical to the state at 6393 keV and not distinct. However, a study of the ^{32}S$(d,t)^{31}$S reaction published in 2013 by Irvine *et al.* [11] provided additional evidence for the existence of a distinct state at 6400 keV as observed by Refs. [16,17], concluding tentatively that its spin was $J = 7/2$, distinct from the state reported in Refs. [20,21]. Recently, Kankainen *et al.* also published a study of the ^{30}P$(d,n)^{31}$S reaction [26], observing a γ-ray transition identified with the state previously reported by Doherty *et al.* at 6393 keV, but no transitions interpreted to be from the 6400-keV state.

Interpreting the energy region surrounding 6400 keV is complicated, and an accurate indirect reaction rate determination requires unambiguous energies, spins, and parities of the resonance states involved in the reaction. As mentioned in Sec. I, experiments that constrain spins and parities, e.g., via β decay, can be very useful toward helping to solve the conundrum. In the present work, we report the detailed results of such a study, including a comprehensive decay scheme including all allowed transitions up to a ^{31}S excitation energy of 6390 keV, comparisons with USD shell-model calculations up to and above that energy level, the properties of a strongly-populated resonance that we initially reported in Ref. [6], discrepancies with the $A = 31$ Nuclear Data Sheets [27], and insight into some of the spin and parity ambiguities arising from the conflicting reports of Refs. [20,21] and [17].

III. EXPERIMENT

The present work describes a measurement of the β-delayed γ decay of ^{31}Cl, one of a program of recent experiments performed at the National Superconducting Cyclotron Laboratory to investigate the sd shell using the β decays of

neutron-deficient nuclides produced by projectile fragmentation [6,28–34]. The experimental procedure has been discussed briefly in prior publications [6,32], but here we present a more detailed description of the procedure and experimental setup.

A beam of stable ^{36}Ar at an energy of 150 MeV per nucleon and a beam current of 75 p nA was produced using the NSCL's ECR ion souce and the Coupled Cyclotron Facility's K500 and K1200 cyclotrons. This beam was then fragmented on a ^{9}Be target of thickness 1627 mg/cm^2 to produce a cocktail beam of various nuclides. The A1900 fragment separator [35] was used to purify the beam and minimize contaminants while maximizing the intensity of the desired isotope. Although the main experimental goal was the study of ^{31}Cl decay, the A1900 was tuned to produce beams composed primarily of both ^{32}Cl and ^{31}Cl beams in succession. The ^{32}Cl beam was used for calibrations, which will be discussed in more detail in Sec. IV. Approximately six hours of ^{32}Cl data were taken; this was sufficient for calibration purposes for our ^{31}Cl data and produced a ^{32}Cl β-delayed γ-ray data set that will be presented in a forthcoming report [36].

To purify both the ^{32}Cl and ^{31}Cl even further, the Radio Frequency Fragment Separator (RFFS) [37] was used downstream of the A1900. Here a time-varying electric field synchronized with the cyclotron RF was used to deflect contaminant ions and produce very pure beams of ^{32,31}Cl. Beam purity was measured using a pair of 300-μm-thick semiconducting Si PIN detectors, located approximately one meter upstream of the experimental setup. Both the energy loss in the PIN detectors and the time of flight between a scintillator located at the focal plane of the A1900 and the PIN detectors were used for particle identification. Because of the high intensities of both the ^{32}Cl and ^{31}Cl beams, the detectors could not reside continuously in the beamline; instead, they were affixed to a pneumatic drive and were inserted into the beamline periodically to perform checks of the beam composition while the beam intensity was attenuated to prevent the deterioration of the PINs via radiation damage.

Data for ^{32}Cl and ^{31}Cl were taken over approximately 6 hours and 36 hours, respectively. The maximum respective rates and purities for the two isotopes were 3.3×10^4 pps at 99% purity (^{32}Cl) and 9000 pps at 95% purity (^{31}Cl). The most intense radioactive contaminants of the ^{31}Cl beam were found to be ^{24}Na (≈2%) and ^{29}P (≈1.5%); a particle identification plot is shown in Fig. 1.

The setup used to measure β decays consisted of a central scintillator of BC408 plastic with dimensions 51 × 51 × 25 mm surrounded by the Clovershare Array of high-purity germanium detectors. The scintillator was mounted in an aluminum housing with an entrance window of aluminized mylar, and optically coupled to a photomultiplier tube (PMT). Incoming ions were implanted into the scintillator, depositing energy and decaying after a time ($T_{1/2}(^{31}Cl) = 190(1)$ ms [13]). The scintillator was used to record the time of an implant or decay, allowing for coincidence gating on β-decay events, including ^{31}Cl.

The Clovershare array consists of nine high-purity germanium "clover" detectors, each housing four semiconducting germanium crystals packed in a square clover-like formation within one cryostat, dimensions ≈10 cm × 10 cm × 10 cm.

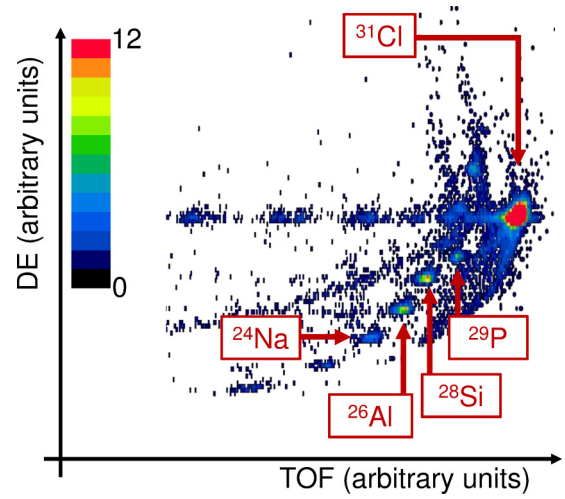

FIG. 1. Particle identification plot showing ^{31}Cl and strongest contaminants. Time of flight between the A1900 focal plane and the Si PIN detector is plotted on the horizontal axis while energy loss in the PIN detector is plotted on the vertical axis. The color scale denotes number of ions, with higher number of ions higher on the scale.

The clover detectors were arranged in two concentric "rings" of four detectors each with both rings centered on the beam axis so that the center of the ring was coaxial with the center of the scintillator detector. The downstream ring had an additional detector centered on the beam axis and coaxial with the scintillator detector. A mechanical design drawing of the clover array is shown in Fig. 2 and a simple schematic showing the detail of the β counter relative to the clover array is shown in Fig. 3. The upstream and downstream rings of clover detectors

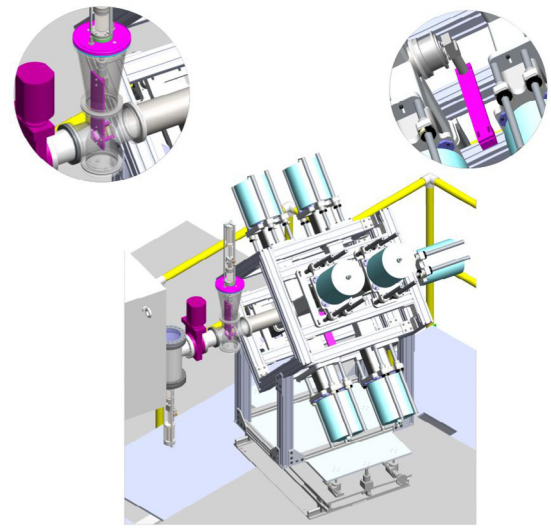

FIG. 2. Computer-aided design drawing of the experiment setup, including the pneumatic drive attached to the PIN detectors (left inset), the central scintillator which was attached to the clover frame by a metal arm (right inset), and the full clover frame with all nine clover detectors (bottom). The liquid nitrogen dewars for the clovers are shown protruding from the clover frame, and the clover detectors themselves can be seen as the rectangular extensions into the center of the array.

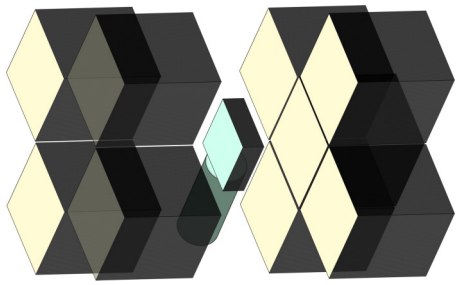

FIG. 3. Simple schematic showing the relative positions of the central scintillator and the surrounding germanium clover detectors (solid angle 6.8 sr). The ^{31}Cl beam particles are implanted from the left into central scintillator, which detects the β particles. The subsequent γ rays emitted by the daughter ^{31}S nucleus are detected by the surrounding clover array.

were both arranged to be as close as possible to the scintillator detector, with the scintillator-facing sides of the rings ≈5 cm (upstream) and ≈7.5 cm (downstream) from the center. The solid angle covered by the clover detectors was approximately 6.8 sr. The clovers and scintillator were all held in place by an aluminum frame. Signals from both the scintillator and the clovers were output to the NSCL Digital Data Acquisition System [38]. During the ^{31}Cl portion of the experiment, the average detection rates in both the scintillator and one crystal of the clover situated directly downstream of the scintillator were recorded. The average scintillator rate was ≈17 000 per second (representing implantations, ^{31}Cl decays, ^{31}S daughter decays, etc.), and the average rate recorded in the monitored clover crystal was ≈415 per second (only the clover behind the scintillator was constantly monitored for detection rate, as it represented the clover likely to have the highest rate).

IV. ANALYSIS

A. γ-ray energy and efficiency calibration

As discussed in Sec. III, we produced a beam of ^{32}Cl for calibration purposes. ^{32}Cl β-coincident γ-ray spectra were generated. A detailed precision γ-ray spectroscopy study of ^{32}Cl was published in 2012 [39] which reported ^{32}S γ-ray energies and intensities up to 7189 keV that we employed as calibration standards. We fit several known ^{32}Cl peaks up to 7189 keV in our spectra, then plotted the obtained peak centroids against the energies of those peaks as reported in Ref. [39] and produced an energy calibration curve by fitting the resulting plot. We used a quadratic function for the calibration fit to account for nonlinearities in the gain. Typical quadratic coefficients for the ^{32}Cl energy scale calibration were on the order of 10^{-9} keV, indicating that the nonlinearity was very small.

Using the calibration curve for the ^{32}Cl data, we then performed an energy calibration on a small set of ^{31}Cl data that was obtained close in time to the ^{32}Cl calibration data (about four hours afterwards). Only data that were taken soon after the ^{32}Cl data were used in this preliminary ^{31}Cl calibration, to minimize the effects of long-term gain drifts. We fit several ^{31}S photopeaks in this calibrated ^{31}Cl spectrum to produce an internal set of ^{31}Cl calibration values, to which the remainder of the ^{31}Cl data was gain-matched, producing a ^{31}Cl calibration that did not require extrapolation or reliance on inconsistent ^{31}S literature values. Five of the 36 clover channels were found to exhibit large and sporadic gain drifts that were impractical to correct; these five channels were excluded from the calibration and subsequent analysis.

In order to check this calibration method, we performed an independent calibration using the cascade-crossover method described in Ref. [40]. This method generates a calibration curve that is not dependent on external data beyond the first two points used to produce a low-energy calibration: the extremely well determined room background peaks at 1460.822(6) and 2614.511(10) keV. The calibration was then extended using γ rays within the low-energy region that form a cascade from a high-lying excited state and compared to cascades including high-E γ rays from the same state, allowing for the extension of the calibration to higher energies by repeated iterations of the method. We used this method to verify the accuracy of the ^{32}Cl calibration, and the two methods were found to give consistent results as discussed and quantified below. Consequently, the simpler ^{32}Cl method was exclusively used on the rest of the ^{31}Cl data.

We obtained both the energies and the corresponding statistical uncertainties (one-sigma) from fits of the photopeaks using exponentially modified Gaussian functions of form

$$\frac{N}{2\tau}\exp\left[\frac{\sigma^2}{2\tau^2}+\frac{x-\mu}{\tau}\right]\left(1-\mathrm{erf}\left[\sigma^2+\tau\frac{x-\mu}{\sqrt{2}\sigma\tau}\right]\right), \quad (3)$$

where N is the integral number of counts in the peak, τ is the decay constant of the exponential, σ is the standard deviation of the Gaussian, and μ is the Gaussian centroid. To assess the accuracy of the calibration and assign systematic uncertainties at low energies, we measured the energies of a number of room background peaks known to high precision, and assigned a 0.2-keV blanket systematic uncertainty up to 2.7 MeV based on the variance of the peak centroids around their literature values [41]. Above 2.7 MeV, we measured the excitation energies of various levels using the cascade-crossover method with multiple cascades from the same level and compared the spread in the excitation energy derived from the cascades. Using this method, we produced a widening uncertainty envelope to high energies: 0.2 keV for $E_\gamma < 2.7$ MeV, 0.3 keV for $2.7 < E_\gamma < 4.8$ MeV, and 0.6 keV for $E_\gamma > 4.8$ MeV.

We produced a γ-ray efficiency curve for our data using two sources: a ^{152}Eu calibration source between 250 keV and 1400 keV and the ^{32}Cl data up to 7189 keV. The curve itself was produced using a two-part procedure: the ^{152}Eu was used to create a curve up to 1400 keV. This curve was then extrapolated up to 1547 keV, where the lowest-energy ^{32}Cl photopeak was anchored to the ^{152}Eu curve. The standard relative intensities of the ^{32}Cl photopeaks [39,42] were then used to extend the curve from 1547 to 7189 keV, producing a relative efficiency curve over the entire energy range of our ^{31}Cl data. The specific shape of this curve was an exponential of the form $\epsilon(E) = \exp[\sum_i p_i \ln(E)^i]$, where $\epsilon(E)$ is the efficiency at a given energy E and the exponential contains a polynomial of degree i ($i = 6$ in our analysis) with argument $\ln(E)$, the

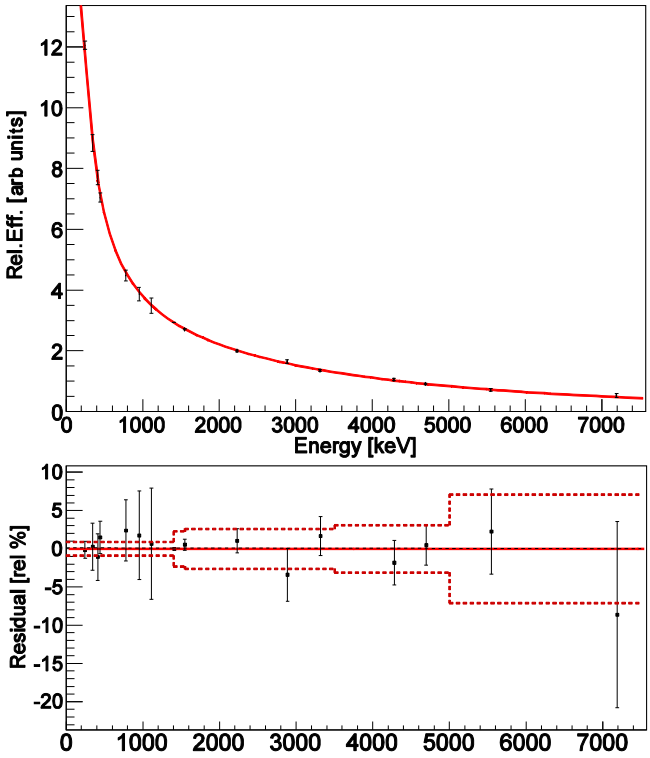

FIG. 4. Upper panel: the smooth relative efficiency curve (red online) generated from fitting the relative efficiencies of the ^{152}Eu and ^{32}Cl data points. Lower panel: residuals of the fit in the upper panel (solid points) and the uncertainty envelope for efficiency adopted across the energy region (dashed lines).

natural logarithm of the energy [43]. Since the lowest γ-ray energy we analyzed was 985 keV, the efficiency curve does not need to turn back over at extremely low γ-ray energies. Both the efficiency curve and uncertainty envelope are shown in Fig. 4.

Although the ^{152}Eu source was absolutely calibrated, our procedure for determining the absolute intensities of the γ rays only required relative efficiencies (see Sec. IV C), so we did not propagate the error due to the calibrated activity of the source. However, our derived intensities still relied on data from Ref. [39] and our own calibration procedure, so it was necessary to propagate uncertainties in the relative efficiency through the intensity calculation. To do this, we first included a flat efficiency uncertainty of 0.7% across all energies based on variations in the photopeak integral as a result of variations in the peak fitting procedure. We then added an uncertainty of 0.2% for $E_\gamma < 1547$ keV from spread between the data points used for calibration and the calibration curve itself in the ^{152}Eu data and a flat 1.4% uncertainty for $E_\gamma > 1400$ keV from the extrapolation of the ^{152}Eu data to 1547 keV. Finally, we included the energy-dependent uncertainty envelope values above $E_\gamma = 1547$ keV taken from the calibration standards in Ref. [39]: 0.4% for $1.5 < E_\gamma < 3.5$ MeV, 1% for $3.5 < E_\gamma < 5$ MeV, and 5% for $E_\gamma > 5$ MeV.

In addition to the systematic uncertainty derived from our efficiency calibration procedures, we also included a uniform

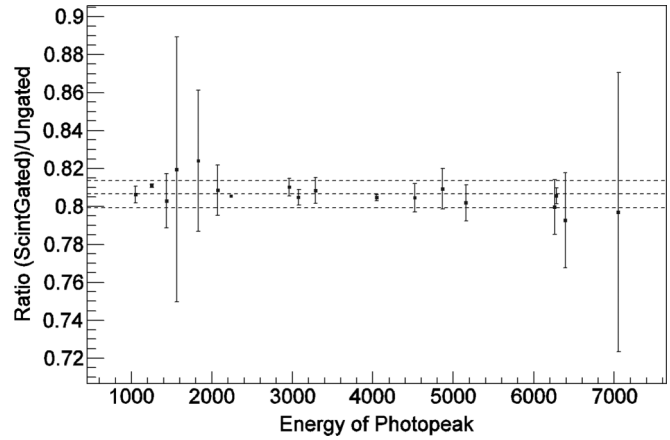

FIG. 5. Ratio of the measured photopeak integral in the scintillator-gated γ-ray spectrum to the measured integral in the ungated spectrum, the mean of the measurements (black dashed line, 80.6%) and the one-sigma envelope denoting the standard deviation of the points about that mean (dashed lines, 0.7%).

1% uncertainty in the efficiencies at all energies to account for γ-γ summing. To arrive at the 1% uncertainty, we simulated the interaction of γ rays in the clover crystals over a range of energies and produced a simulated γ-ray spectrum at each energy simulated. We then integrated each spectrum to produce a total interaction efficiency at that energy (that is, we integrated the entirety of each spectrum produced, not just the photopeak at the energy of the simulated γ ray). This 1% uncertainty was factored into the photopeak intensities used to determine the branching ratios and efficiencies for each transition.

B. $\beta\gamma$ coincidences and β detection efficiency

In order to reduce the contribution from contaminant sources such as room background and spilled beam (beam that was stopped or implanted in places other than the scintillator), we applied a 1-μs timing coincidence window between events in the clover detectors and events in the central scintillator to preferentially select events corresponding to β decays of implanted ions. We found that, when we applied the timing gate and compared the integrals of the gated peaks to the ungated peaks, the timing gate reduced known ^{31}Cl peak integrals by a constant factor, yielding a ratio of timing-gated intensity to ungated intensity of 0.806(7). This ratio was observed for a set of ^{31}Cl peaks over a broad energy range as shown in Fig. 5, and is likely due to the presence of a 3.8-cm-diameter collimator at the end of the beam line and the finite transverse extent of the beam. For the portion of the beam particles that were likely implanted into the collimator instead of the scintillator, the β-detection efficiency in the scintillator is relatively low but the γ-detection efficiency in the Ge array remains essentially the same.

The fact that this ratio is consistent over the entire energy range implies that the efficiency to detect β particles in coincidence with γ rays is essentially constant. We thus used the $\beta\gamma$ coincidence condition to populate a gated γ-ray spectrum for analysis. This spectrum is shown with peak identification in Fig. 6 and it was used to determine γ-ray energies, intensities, and β feedings.

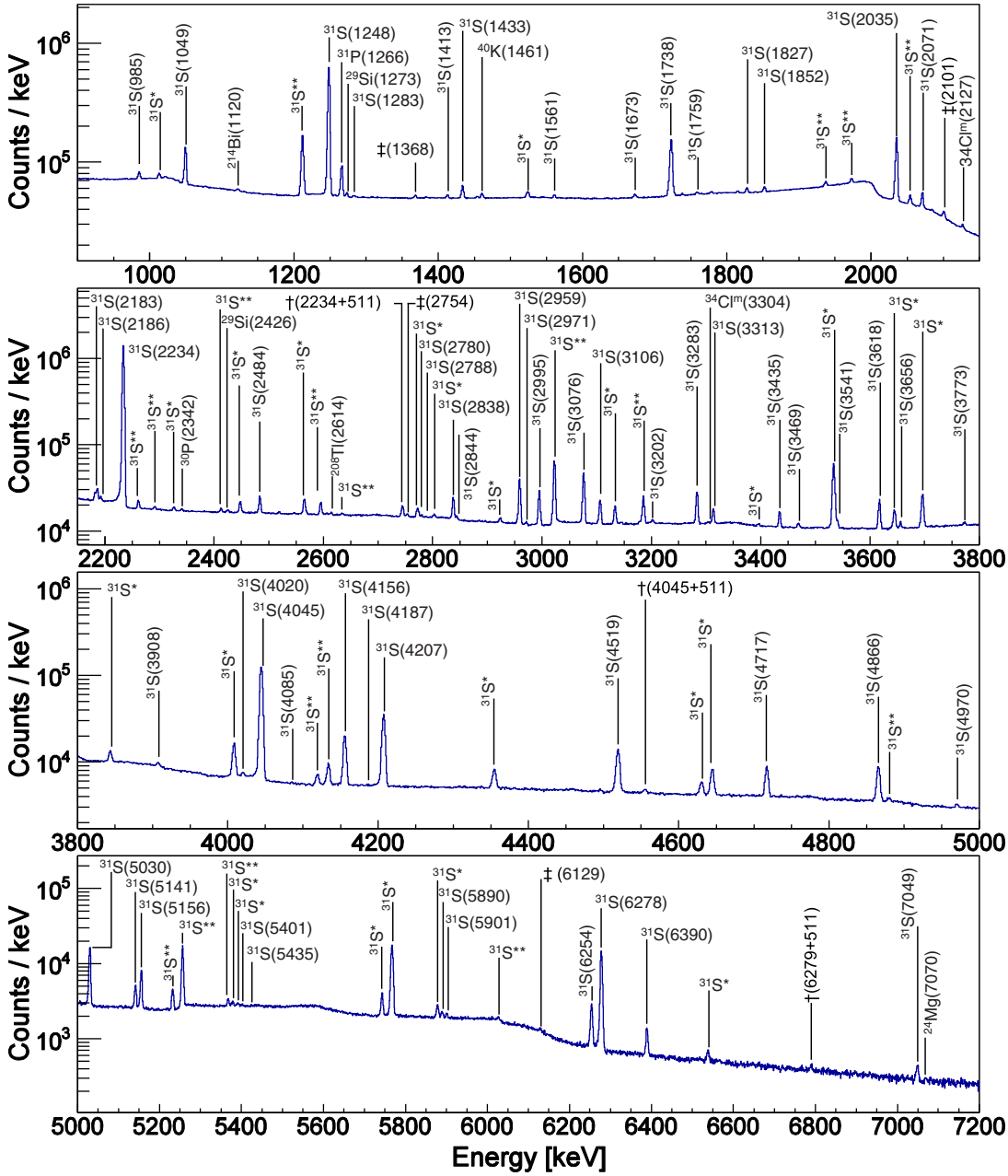

FIG. 6. Cumulative Clovershare spectrum in coincidence with scintillator events showing the assignments for the photopeaks used to construct the ^{31}Cl β decay scheme as well as those for identified contaminants. Each photopeak (black [blue online] line) is labeled by the emitting nucleus and its energy. Peaks labeled with one or two asterisks correspond to single and double escape peaks, respectively. Peaks marked with a single dagger are sum peaks with the summation noted. Peaks marked with a double dagger have multiple contributions.

C. Determination of β feedings and γ-ray intensities

Typically, β-delayed γ-ray spectroscopy experiments measure the β feedings of the nuclear states using the intensities of γ-ray transitions as a proxy. In order to build an experimental decay scheme, it is necessary to determine where in the scheme each transition should be placed, inferring the excitation energies of the nuclear states and making spin and parity arguments in the process. Once all the transitions deexciting a particular nuclear state have been found, the γ branches from that state can be determined, and once all the transitions feeding the state are known, its β-decay branching ratio I_β can be determined as well using the formula

$$\frac{N_{\text{out}} - N_{\text{in}}}{N_\beta} = I_\beta, \tag{4}$$

where N_{out} and N_{in} are the numbers of γ rays deexciting and feeding the level, respectively, and N_β is the total number of β decays. The Gamow-Teller transition strength $B(GT)$ can be determined from the Q value and half-life of the decay, the excitation energy of the state, and the β feeding; the transition strength may then be used [along with a Fermi transition strength $B(F)$ if the state has one] to calculate the reduced

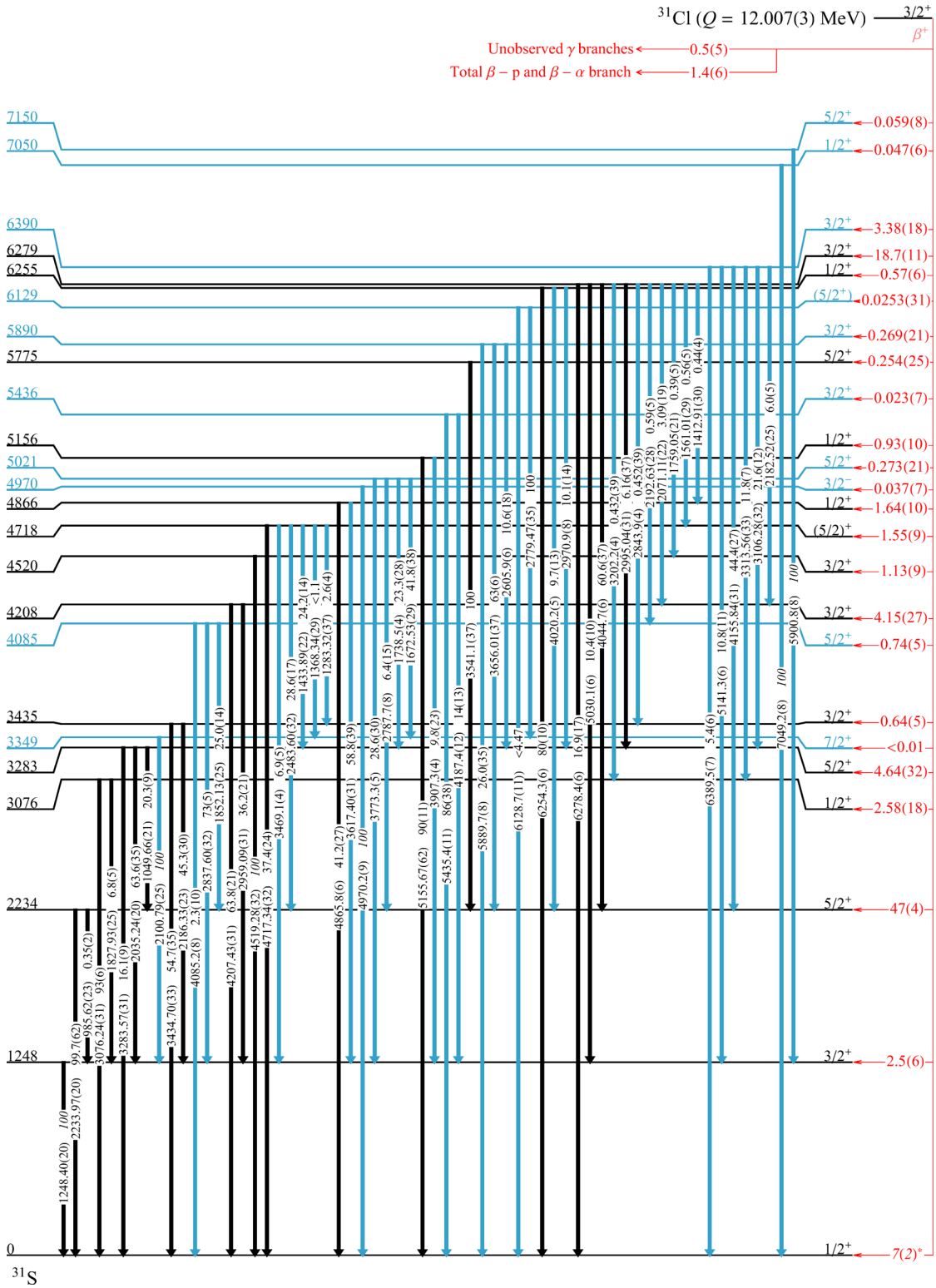

FIG. 7. Comprehensive ^{31}Cl decay scheme produced from the analysis of the present experiment. For each level, the excitation energy rounded to the nearest keV labels the left wing of the level and its spin and parity J^{π} are reported on the right wing. The precise excitation energies E_x of each level are reported in Table I. Each β decay transition is depicted by a light grey (red online) arrow on the right side of the figure and includes its intensity I_β, also reported in Table I. Dark grey (blue online) coloring for a level indicates that the level has not been previously observed in ^{31}Cl β decay. γ-ray transitions between ^{31}S levels are denoted in the table by the vertical arrows. Each transition is labeled by the γ-ray energy E_γ and branching ratio (B.R.), which are both reported in Table I. As with the populated levels, γ transitions which have never been observed in ^{31}Cl β decay before are colored grey (blue online). The scheme also incorporates the adopted branches for β-proton, β-α, and unobserved γ rays. The $*$ labeling the ground state denotes that this branch was adopted from literature.

transition strength $ft_{1/2}$:

$$ft_{1/2} = \frac{C}{[B(F) + (g_V/g_A)^2 B(GT)]} \tag{5}$$

where here $B(GT) = 0$ for pure Fermi transitions and g_A and g_V are the coupling constants for the vector and axial vector decays. Alternatively, the reduced transition strength $ft_{1/2}$ can be calculated from various phase space factors and corrections [44,45]. This reduced transition strength is then a good test of the theoretical nuclear wave functions.

The processes of determining both β feedings and γ-ray intensities were constrained by the fact that the PIN detectors had to be extracted from the beamline for the majority of the experiment. Thus, any normalization to the estimated number of implanted ^{31}Cl ions would be subject to systematic uncertainties that are difficult to quantify. Instead, we circumvented calculations using the measured number of β decays and performed a normalization based on the β feedings (by requiring that they sum to 100%) and absolute γ-ray intensities per β decay entirely from the measured γ-ray photopeak intensities.

Our normalization procedure required us to first adopt values for unseen β-decay branches. Following Ref. [12] we adopted a 7(2)% β feeding for the ground state; this value is based on the ^{31}Si β decay branch to the ^{31}P ground state, the mirror process for ^{31}Cl β feeding of the ^{31}S ground state. This value was corroborated by a 7.9% ground-state β feeding in our USD shell-model calculation (Sec. V F). The β-α and β-proton branch we adopted, 1.4(6)%, was based on improvements to the value used in Refs. [12] by [13] and our shell-model calculations.

We estimated a conservative 0.5(5)% branch for unseen γ rays based on comparisons between the γ branches we expected from our shell-model calculations and what we actually observed. We summed these unseen branches to a total 8.9(22)% for unobserved β feeding and, reasoning that the remaining β feeding was distributed across the levels from which γ decay was observed, used the remaining 91.1(22)% of the β feeding to normalize the total feeding for all observed levels. The γ-ray intensities were then determined from the β feeding values and the γ-decay branching ratios. The uncertainties on these intensity values factored in the statistical uncertainties (derived from the peak fit), the uncertainties in the adopted unobserved γ branches (essentially a purely systematic uncertainty), the statistical and systematic uncertainties of the relative γ-ray intensities, and the uncertainties propagated through the normalization of the γ intensities for each energy level (including the above-mentioned 1% uncertainty due to summing, 0.7% uncertainty from variations in the peak-fitting procedure, and energy-dependent uncertainties from the efficiency calibration, both those from our own procedure and those adopted from Ref. [39]). Uncertainties to the observed efficiency-corrected γ-ray intensities from the various unrelated sources were added linearly to produce a total observed uncertainty $dI_{\gamma,obs}$.

The absolute γ-ray intensity for a given transition i de-exciting a state n was then calculated as shown here, with ground-state β branch $I_{\beta,grd}$, β-proton branch $I_{\beta+p}$, unseen γ branch $I_{\gamma,unsn}$, the sum of all observed intensities for the γ rays i de-exciting the state $\sum_i I_{\gamma,obs,i}$, and the sum of the beta intensities over all states $\sum_n I_{\gamma\beta,n}$:

$$I_{\gamma,abs,i} = I_{\gamma,obs,i} \frac{I_{\beta,grd} + I_{\beta+p} + I_{\gamma,unsn}}{\sum_i I_{\gamma,obs,i} + \left(\sum_n I_{\gamma\beta,n} - I_{\gamma\beta,n}\right)}, \tag{6}$$

The uncertainty on this absolute γ-ray intensity was then calculated through standard error propagation for the above quantities, using the relevant values for $dI_{\gamma,obs,i}$, $dI_{\beta,grd}$, $dI_{\beta+p}$, $dI_{\gamma,unsn}$, and $dI_{\gamma\beta,n}$. A more thorough discussion of error propagation can be found in Ref. [46].

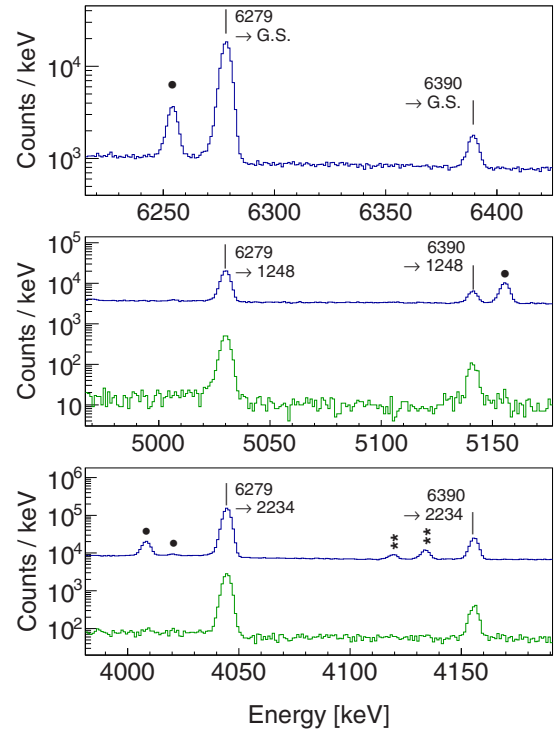

FIG. 8. Sample portions of the $\beta\gamma$ and $\beta\gamma\gamma$ coincidence spectra. The top panel shows $\beta\gamma$ transitions (black [blue online] line) from both the isobaric analog state at 6279 keV and the $3/2^+$ state at 6390 keV to the ground state. The middle and bottom panels also include $\beta\gamma\gamma$ transitions (grey [green online] line) from these two states to the first excited state at 1248 keV (middle panel) and the second excited state at 2234 keV (bottom panel), gated on the first and second excited states, respectively. Other ^{31}Cl peaks are marked with a dot, while double escape peaks are marked with two asterisks.

D. $\beta\gamma\gamma$ coincidences

In addition to using $\beta\gamma$ coincidences to build the decay scheme, the high statistics of this experiment and the high granularity of the Clovershare array allowed us to sort our data using $\beta\gamma\gamma$ gating between the scintillator and multiple clover crystals as well. This allowed us to confirm γ cascades directly, enabling a more confident determination of the decay scheme. Samples of the $\beta\gamma\gamma$ spectra are shown in Fig. 8. To address the potential contribution of accidental coincidences to the spectra, we calculated two estimates: one for the rate of chance coincidences between the scintillator and the clovers and one for coincidences between the clovers themselves.

Using the 1-μs time window and the scintillator and clover rates reported above (17 000 and 415, respectively) [40], we calculated rates of ≈14 scintillator-clover chance coincidences per second and ≈0.34 clover-clover chance coincidences per second. Both rates only factor in a single clover crystal, as we only measured the ongoing rate in one clover crystal for the clover likely to have the highest rate, and should additionally be understood to be upper limits for these estimates.

V. EXPERIMENTAL RESULTS AND DISCUSSION

As shown in Figs. 6 and 7, the present experiment has expanded greatly on previous ^{31}Cl β decay work. We have observed a total of 62 ^{31}S γ-ray transitions—over twice as many as the 29 transitions reported in the 2012 $A = 31$ Nuclear Data Sheets [27] and in the most recent ^{31}Cl β-decay study [13], which reported 27. In addition, we observed β-decay transitions to ten ^{31}S levels previously unobserved in ^{31}Cl β decay, including the tentative first observation of a forbidden transition in this decay.

A. 6390-keV state

Through six new primary branches, we observed the γ-ray deexcitation of a new ^{31}S state at $E_x = 6390.2(7)$ keV, as previously reported in Ref. [6]. Neither the β feeding nor the γ-decay branching of the state match our USDB predictions [47] without isospin mixing, and the state's β feeding was abnormally high for a Gamow-Teller transition to a state at such a high energy. By computing the Fermi strengths B for both the $T = 3/2$ ^{31}S IAS at 6279.0(6) keV and this state, it was discovered that the two states were mixing isospin strongly. The mixing allowed for an unambiguous spin and parity identification of $J^\pi = 3/2^+$ for the 6390-keV state. The positive identification of the state has implications for the ^{30}P$(p,\gamma)^{31}$S reaction rate in the astrophysical environment of a classical nova outburst; these findings are discussed in Ref. [6]. The strong population in ^{31}Cl β decay also opens up a potential method to measure Γ_p/Γ. Excitation energies, γ-decay energies, and β feedings of the two states are summarized in Table I.

B. Potential forbidden transitions

We observed a new γ ray at a photopeak energy of $E_\gamma = 4970.2(9)$ keV (reported in Table I). It was not observed in coincidence with any other γ ray, and the ratio of its scintillator-gated intensity to its ungated intensity was found to be 0.85(15), consistent with the average ratio of 0.806(7), suggesting a possible origin from ^{31}Cl β decay. The $A = 31$ Nuclear Data Sheets (NDS) [27] report a state at $E_x = 4971(3)$ based on a number of nuclear reaction experiments [48–53] with a spin and parity assignment $J^\pi = 3/2^-$; none of these experiments, however, measured γ-ray transitions. We calculated a β feeding for this level of 0.037(7)%, which corresponds to a $\log(ft_{1/2})$ value of 6.61 (typical $\log(ft_{1/2})$ values for first-forbidden transitions are > 5.9 for $\Delta J = 0,1$ [54]). We have therefore tentatively labeled the state as $J^\pi = 3/2^-$ in the decay scheme, in concert with the assignment from Ref. [27], and surmise that it may be fed by the first-forbidden β decay of ^{31}Cl. Two other states, at 5436 and 6129 keV, have $\log(ft_{1/2})$ values > 6.0, but as we were able to match those states to sd shell-model states of positive parity, we do not argue that they are the result of forbidden transitions.

Although no γ rays have been observed to date feeding or deexciting this state, and we did not observe any feeding from higher-energy states or coincident γ rays, it is possible that the finite intensity deduced for this state is due in part to unseen weak γ feeding from higher-lying excited states, and that the apparent intensity is thus higher than the true intensity, due to the Pandemonium effect [55]. It is difficult to quantify the extent of any such effect on the apparent feeding of this level. We therefore present our observed feeding as a tentative assessment of the level's feeding. Regardless, the deexciting γ ray is the first measured γ deexcitation of the state, and the calculated excitation energy of 4970.7(9) keV is more precise than the NDS reported value.

We also observed evidence for the population of a state with a spin and parity of $J^\pi = 7/2^+$. Direct population of this state by β decay would be surprising because it would have to proceed via a second-forbidden transition. Two γ rays with energies of 2100 and 1673 keV were observed in coincidence with one another; these energies together sum to 3773 keV, 1248 keV less than the excitation energy of a known state at 5021 keV. The 2100-keV peak was also observed to be in coincidence with the 1248-keV γ-ray transition from the first excited state. After further analysis, including consideration of our shell-model calculations, we found that the 5021-keV state is expected to have four primary γ branches: to the 1248-keV state (we observed a transition from the state at 5021 keV to the first excited state), to the 2234-keV state, to the 3283-keV state, and to a $J^\pi = 7/2^+$ state at a theoretically predicted energy of 3477 keV. We thus considered the 2100-keV γ to be deexciting a $7/2^+$ state at excitation energy $E_x = 3349.30(32)$ keV, and the 1673-keV γ to be feeding it via deexcitation of the 5012-keV state. These, along with other relevant γ rays that feed the state, are reported in Table I. The ^{31}Cl β-decay transition to the $7/2^+$ state at 3349 keV would be a second-forbidden transition that should be strongly suppressed. Using our data, we calculated a β feeding upper limit for this state of $I_\beta < 0.01$ (C.L 90%).

C. Peaks with multiple contributions

As shown in Fig. 6, several peaks were found to have contributions from more than one source: the 1368-keV γ ray feeding the 3349-keV level, the 2100-keV γ ray deexciting it, as well as two photopeaks corresponding to transitions of energies 2779 and 6129 keV, both deexciting a state at 6129 keV. For the 3349- and 2100-keV peaks, the contaminant sources were found to be background emissions (^{24}Al and ^{24}Na β decay and room background), whereas the contaminant source for the 6129-keV peak was determined to likely be ^{16}O produced by nuclear reactions between the beam and the scintillator. To treat these anomalies and determine the accurate γ-ray intensities, we employed various techniques to ascertain the strength of contaminant contributions to the peaks in question, including background/contaminant decay intensity calculations utilizing multiple-peak fits, and simulations of

TABLE I. ^{31}S level excitation energies E_x, β-decay intensities $I_{\beta\gamma}$ and corresponding $\log(ft)$ values, and transitions from each level observed in the β decay of ^{31}Cl (the designation J^π_n denotes the nth state of a given spin and parity). Also included for each transition are the observed γ-ray deexcitation energies E_γ, relative γ-ray branching ratios (B.R.), and absolute γ-ray intensity per 100 β decays, I_γ. "†" denotes an upper limit on the ^{31}Cl contribution to an observed transition (C.L. 90%). The β feeding and $\log(ft)$ value of the 4970-keV level (marked $*$) are tentative; see the discussion in Sec. V B.

E_x (keV)	$I_{\beta\gamma}$ (%)	$\log(ft)$	Transition	E_γ (keV)	B.R.(%)	I_γ (%)
1248.43(20)	2.5(6)	5.77(10)	$3/2^+_1 \rightarrow 1/2^+_1$	1248.40(20)	100	12.3(5)
2234.06(20)	47(4)	4.28(7)	$5/2^+_1 \rightarrow 1/2^+_1$	2233.97(20)	99.7(62)	53.2(27)
			$5/2^+_1 \rightarrow 3/2^+_1$	985.62(23)	0.35(2)	0.187(9)
3076.40(31)	2.58(18)	5.33(4)	$1/2^+_2 \rightarrow 1/2^+_1$	3076.24(20)	93(6)	2.82(14)
			$1/2^+_2 \rightarrow 3/2^+_1$	1827.93(25)	6.8(5)	0.205(14)
3283.76(31)	4.64(32)	5.02(4)	$5/2^+_2 \rightarrow 1/2^+_1$	3283.57(31)	16.1(9)	1.11(6)
			$5/2^+_2 \rightarrow 3/2^+_1$	2035.24(20)	63.6(35)	4.38(22)
			$5/2^+_2 \rightarrow 5/2^+_1$	1049.66(21)	20.3(9)	1.40(5)
3349.30(32)	<0.01	>7.7	$7/2^+_1 \rightarrow 3/2^+_1$	2100.79(25)	100	0.076(14)
3434.90(33)	0.64(5)	5.84(4)	$3/2^+_2 \rightarrow 1/2^+_1$	3434.70(32)	54.7(35)	0.420(24)
			$3/2^+_2 \rightarrow 3/2^+_1$	2186.33(33)	45.3(30)	0.348(21)
4085.4(8)	0.74(5)	5.59(3)	$5/2^+_3 \rightarrow 1/2^+_1$	4085.2(8)	2.3(10)	0.019(8)
			$5/2^+_3 \rightarrow 3/2^+_1$	2837.60(32)	73(5)	0.614(34)
			$5/2^+_3 \rightarrow 5/2^+_1$	1852.19(25)	25.0(14)	0.211(14)
4207.7(31)	4.15(27)	4.81(4)	$3/2^+_3 \rightarrow 1/2^+_1$	4207.43(31)	63.8(21)	3.12(18)
			$3/2^+_3 \rightarrow 3/2^+_1$	2959.09(31)	36.2(21)	1.77(9)
4519.63(32)	1.13(9)	5.278(35)	$3/2^+_4 \rightarrow 1/2^+_1$	4519.28(32)	100	1.20(7)
4717.72(32)	1.55(9)	5.077(34)	$5/2^+_4 \rightarrow 1/2^+_1$	4717.34(32)	37.5(24)	0.618(37)
			$5/2^+_4 \rightarrow 3/2^+_1$	3469.13(31)	6.9(5)	0.113(8)
			$5/2^+_4 \rightarrow 5/2^+_1$	2483.60(22)	28.7(17)	0.472(26)
			$5/2^+_4 \rightarrow 5/2^+_2$	1433.89(22)	24.3(14)	0.399(22)
			$5/2^+_4 \rightarrow 7/2^+_1$	1368.34(29)	$\leqslant$1.1	$\leqslant$0.018
			$5/2^+_4 \rightarrow 3/2^+_2$	1283.32(37)	2.6(4)	0.043(7)
4866.2(6)	1.64(10)	5.003(35)	$1/2^+_3 \rightarrow 1/2^+_1$	4865.8(6)	41.2(27)	0.71(4)
			$1/2^+_3 \rightarrow 3/2^+_1$	3617.40(31)	58.8(39)	1.01(6)
4970.7(9)	0.037(7)	6.62(9)*	$3/2^-_1 \rightarrow 1/2^+_1$	4970.2(9)	100	0.037(7)*
5021.9(5)	0.273(21)	5.73(4)	$5/2^+_5 \rightarrow 3/2^+_1$	3773.2(5)	28.6(30)	0.078(7)
			$5/2^+_5 \rightarrow 5/2^+_1$	2787.7(8)	6.4(15)	0.0173(39)
			$5/2^+_5 \rightarrow 5/2^+_2$	1738.52(36)	23.3(28)	0.063(7)
			$5/2^+_5 \rightarrow 7/2^+_1$	1672.53(29)	41.8(38)	0.114(9)
5156.1(6)	0.93(10)	5.15(5)	$1/2^+_4 \rightarrow 1/2^+_1$	5155.7(6)	90(11)	0.84(8)
			$1/2^+_4 \rightarrow 3/2^+_1$	3907.3(4)	9.8(23)	0.091(8)
5435.9(9)	0.023(7)	6.66(14)	$3/2^+_5 \rightarrow 1/2^+_1$	5435.4(9)	86(38)	0.020(7)
			$3/2^+_5 \rightarrow 3/2^+_1$	4187.4(15)	14(5)	0.0034(7)
5775.4(4)	0.254(25)	5.49(4)	$5/2^+_6 \rightarrow 5/2^+_1$	3541.10(27)	100	0.254(21)
5890.3(8)	0.269(21)	5.42(4)	$3/2^+_6 \rightarrow 1/2^+_1$	5889.7(8)	26.0(35)	0.070(9)
			$3/2^+_6 \rightarrow 5/2^+_1$	3656.01(37)	63(6)	0.170(12)
			$3/2^+_6 \rightarrow 5/2^+_2$	2605.9(5)	10.6(18)	0.029(5)
6129.3(10)	0.0253(31)	6.35(6)	$5/2^+_7 \rightarrow 1/2^+_1$	6128.7(10)	$\leqslant$ 4.47†	$\leqslant$ 0.0012†
			$5/2^+_7 \rightarrow 7/2^+_1$	2779.5(6)	100	0.0253(18)
6255.0(6)	0.57(6)	4.94(5)	$1/2^+_5 \rightarrow 1/2^+_1$	6254.3(6)	80(10)	0.46(4)
			$1/2^+_5 \rightarrow 5/2^+_1$	4020.2(5)	9.7(13)	0.055(6)
			$1/2^+_5 \rightarrow 5/2^+_2$	2970.9(4)	10.1(14)	0.058(6)
6279.0(6)	18.7(11)	3.42(3)	$3/2^+_7 \rightarrow 1/2^+_1$	6278.4(6)	16.9(17)	3.15(30)
			$3/2^+_7 \rightarrow 3/2^+_1$	5030.1(6)	10.4(10)	1.94(18)
			$3/2^+_7 \rightarrow 5/2^+_1$	4044.7(30)	60.6(37)	11.3(6)
			$3/2^+_7 \rightarrow 1/2^+_2$	3202.2(4)	0.432(39)	0.081(7)
			$3/2^+_7 \rightarrow 5/2^+_2$	2995.04(31)	6.16(37)	1.15(6)

TABLE I. (*Continued.*)

E_x (keV)	$I_{\beta\gamma}$ (%)	log(ft)	Transition	E_γ (keV)	B.R.(%)	I_γ (%)
			$3/2^+_7 \rightarrow 3/2^+_2$	2843.9(4)	0.452(39)	0.084(7)
			$3/2^+_7 \rightarrow 5/2^+_3$	2192.63(28)	0.59(5)	0.110(9)
			$3/2^+_7 \rightarrow 3/2^+_3$	2071.11(22)	3.09(19)	0.577(32)
			$3/2^+_7 \rightarrow 3/2^+_4$	1759.05(34)	0.39(5)	0.072(8)
			$3/2^+_7 \rightarrow 5/2^+_4$	1561.01(29)	0.56(5)	0.104(8)
			$3/2^+_7 \rightarrow 1/2^+_3$	1412.91(30)	0.44(4)	0.082(7)
6390.2(7)	3.38(18)	4.112(33)	$3/2^+_8 \rightarrow 1/2^+_1$	6389.5(7)	5.4(6)	0.181(18)
			$3/2^+_8 \rightarrow 3/2^+_1$	5141.3(6)	10.8(11)	0.368(36)
			$3/2^+_8 \rightarrow 5/2^+_1$	4155.84(31)	44.4(27)	1.51(9)
			$3/2^+_8 \rightarrow 1/2^+_2$	3313.56(33)	11.8(7)	0.401(22)
			$3/2^+_8 \rightarrow 5/2^+_2$	3106.28(31)	21.6(12)	0.734(39)
			$3/2^+_8 \rightarrow 3/2^+_2$	2182.52(25)	6.0(5)	0.210(16)
7050.0(8)	0.047(6)	5.66(6)	$1/2^+_6 \rightarrow 1/2^+_1$	7049.2(8)	100	0.047(5)
7149.8(9)	0.059(8)	5.51(6)	$5/2^+_{10} \rightarrow 3/2^+_1$	5900.8(8)	100	0.059(7)

^{16}O production in the scintillator. The intensities reported in the present work represent just the contributions from ^{31}Cl β decay. A more detailed discussion of the techniques used to isolate the ^{31}Cl contribution can be found in Ref. [46].

D. Comparison to the Nuclear Data Sheets and previous ^{31}Cl β-decay work

We generally see very good agreement between our results and both the $A = 31$ NDS [27] and previous literature. However, several states reported in the NDS between $E_x = 5$ MeV and $E_x = 8$ MeV to be populated in ^{31}Cl β decay were *not* observed in our analysis. The excitation energies of these states reported in the β decay scheme of the NDS are 5408.2, 5786.2, 6420.7, 7280.0 7416.8, 7631.8, and 7644.5 keV. The states at 5786, 6421, 7280, 7417, 7632, and 7645 keV are from tentative assignments made in the previous ^{31}Cl β-delayed γ-decay study [13], but our experiment was much more sensitive and did not exhibit evidence for the peaks corresponding to these states (Fig. 9). Therefore, we attribute them to contaminants in the experiment of Ref. [13] and omit them from our normalization and decay scheme. The 5408-keV state was also reported in Ref. [13] and previously in Ref. [51]; the latter assigned tentative spins of $J = (3/2,5/2,7/2)$, but as we again did not observe the peak, we consider $J^\pi = (3/2,5/2)^+$ to be unlikely and have omitted the peak from our normalization and decay scheme.

The $A = 31$ NDS also report a transition from the state at 3076 keV to the state at 2234 keV, based on the reports of Refs. [13] and [56], but note in their decay scheme that the transition was not included in the least-squares fit that resulted in the quantities reported in the table. Ref. [13] assigned the transition an absolute γ intensity per 100 β decays of $I_\gamma = 1.1(1)\%$, implying that the peak should be stronger than the nearby 985-keV γ ray marking the transition between the 2234- and 1248-keV states, which is assigned an absolute intensity of only 0.2(1)%. However, despite observing the 985-keV γ ray, we did not observe a photopeak at 845 keV in our β-delayed γ-ray spectrum or in the 2234-keV coincidence spectrum. After fitting this region, we obtained an upper limit on the intensity of this transition of $I_\gamma \leqslant 0.018(4)\%$ (C.L. 90%), and have omitted it from our normalization and decay scheme.

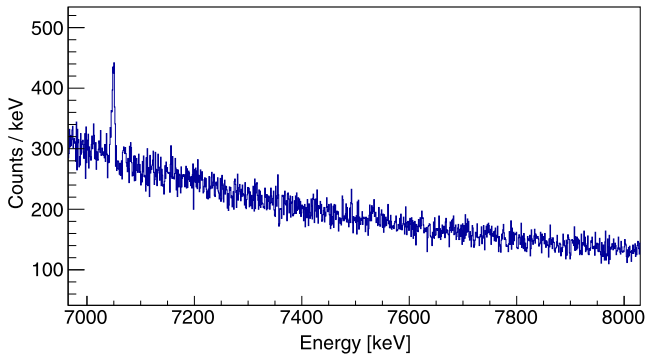

FIG. 9. Cumulative Clovershare $\beta\gamma$ spectrum from 7 MeV to 8 MeV in coincidence with scintillator events. The only significant peak in the spectrum, at 7049 keV, corresponds to a transition from the second $T = 3/2$ ^{31}S state to the ground state.

E. Spin and parity constraints

As discussed, the spins and parities of several important resonance states in the ^{30}P(p,γ)^{31}S Gamow window are ambiguous, due in part to discrepancies between assignments from different experiments [17,20,21]. Since ^{31}Cl β decay preferentially populates $J^\pi = 1/2^+, 3/2^+$, and $5/2^+$ states, we can compare our assignments to those from previous studies and comment on the likelihood that their spin and parity assignments are accurate.

Reference [17], for example, reports states at 6328.6(9) and 6356.1(9) keV, with $J^\pi = 1/2^+$ and $3/2^+$, respectively. Reference [21], however, assigns these states spins and parities of $3/2^-$ and $5/2^-$, respectively. The fact that that these levels were not observed in our experiment provides evidence that the spin and parity assignments of Ref. [21] are more likely to be accurate for these states due to β-decay selection rules.

Reference [17] also reports a number of other states that might be populated in ^{31}Cl β decay, but are absent: a level at 6719.9(9) keV with $J = 5/2$, a level at 6749.0(9) keV with $J^\pi = 3/2^+$, a level at 6936.7(17) keV with $J^\pi = (1/2\text{–}5/2)^+$, a level at 6959.6(16) keV with $J^\pi = 1/2^+$, and a level at 7033.5(13) keV with $J^\pi = (1/2\text{–}5/2)^+$. These higher-energy resonances decay primarily via proton emission [51], so the lack of observation in our data is not surprising, given that our experiment was not sensitive to the delayed proton branch.

We also observe a few discrepancies with Ref. [21]. The level reported in Ref. [21] at $E_x = 4527.8(2)$ keV is given a J^π assignment of $3/2^+$. We did not observe any state at this energy; the closest candidate is the state at $E_x = 4519.63(32)$ keV, which we also assigned $J^\pi = 3/2^+$. Reference [21] also reported a state at $E_x = 4710.1(8)$ with $J^\pi = 5/2^+$. We again did not observe a state at this energy, but instead have identified a $5/2^+$ state at the nearby energy $E_x = 4717.72(32)$ keV. We did not observe the $5/2^+$ state Ref. [21] reports at 5401.5(8) keV or the $5/2^+$ state at 5518.3(3) keV, and the closest state we observed to these energies, at 5435.9(9) keV, was assigned $J^\pi = 3/2^+$. We also observed a state at 5775.4(4) keV, to which we have assigned a spin and parity of $5/2^+$, but which Ref. [21] did not report. Our experiment should be sensitive enough to observe all allowed β-decay transitions to bound states, but there are not enough shell-model levels to support both the assignments of Doherty *et al.* and the present work, implying that further study is required.

Perhaps the most interesting point of comparison between the present work and Ref. [21] is the states at 6390 keV [6,21]. Reference [21] reports a state at the nearby energy of 6392.5(2) keV and assigns it a spin and parity of $5/2^+$, based on the angular distribution of the transition observed and a proposed mirror assignment with the 6461-keV ^{31}P state. We did not observe this state, and the closest $5/2^+$ state to the 6390-keV state predicted by our shell-model calculations is $\approx$300 keV higher. The $3/2^+$ assignment for our 6390-keV state is based on the observation of isospin mixing with the nearby isobaric analog state [6]—a strong constraint on spin—and the observed γ-ray branchings are incompatible. Our nonobservation of the $5/2^+$ state at 6392.5 keV implies that its β feeding would have to be sufficiently low that its photopeaks are overwhelmed by the nearby photopeaks from the 6390-keV state. Also worth noting is the observation by Ref. [13] of a γ-ray peak at 6389.7(11) keV in another ^{31}Cl β-decay experiment [13] with a similar intensity to that observed in the present work. The authors of Ref. [13] did not place the corresponding γ-ray transition in their ^{31}Cl β-decay scheme.

F. Comparison to shell model

As discussed in Sec. I, comparison between our experimental β feedings and γ branchings and the results of USD nuclear shell-model calculations was made to enhance the spin and parity arguments. We initially used USDB calculations for this analysis but, as discussed in Ref. [6], eventually developed the "USDE" interaction, which is similar to USDB but fit only on excitation energies (excluding binding energies). Every observed level up to the level at 6390 keV was then matched with a particular shell-model level from the USDE calculations; the energy and log(ft) comparisons are reported in Table II.

TABLE II. Comparison between observed ^{31}S level excitation energies (all energies are in keV) and log(ft) values up to 6390 keV and their corresponding USDE (marked E) and USDB (marked B) shell-model theoretical values. For the $3/2^+$ levels, the USDE and USDB calculation provided both a Gamow-Teller transition strength and a Fermi transition strength; these have been added to give the shell-model result (marked with an asterisk).

j^π	$E_{x_{exp}}$	log(ft)$_{exp}$	E_{x_E}	log(ft)$_E$	E_{x_B}	log(ft)$_B$
$1/2^+_1$	0 (g.s)	5.578(26)	0 (g.s)	5.52	0 (g.s)	5.52
$3/2^+_1$	1248	5.77(10)	1212	5.49*	1195	5.29*
$5/2^+_1$	2234	4.28(7)	2279	4.32	2297	4.30
$1/2^+_2$	3076	5.33(4)	3230	5.45	3187	5.43
$5/2^+_2$	3284	5.02(4)	3304	4.86	3318	4.96
$3/2^+_2$	3435	5.84(4)	3600	6.30*	3624	6.00*
$5/2^+_3$	4085	5.59(3)	4230	5.53	4269	5.35
$3/2^+_3$	4208	4.81(4)	4343	4.84	4336	4.82
$3/2^+_4$	4520	5.278(35)	4607	5.96*	4652	5.59
$5/2^+_4$	4718	5.077(34)	4831	5.08	4832	5.12
$1/2^+_3$	4866	5.003(35)	4911	4.65	4948	4.58
$5/2^+_5$	5022	5.73(4)	5124	5.67	5155	5.52
$1/2^+_4$	5156	5.15(5)	5384	6.56	5502	6.23
$3/2^+_5$	5436	6.66(14)	5710	5.74*	5764	6.00*
$5/2^+_6$	5775	5.49(4)	5741	5.68	5772	5.58
$3/2^+_6$	5890	5.42(4)	6102	4.98*	6199	5.20*
$5/2^+_7$	6129	6.35(6)	6345	6.06	6278	5.72
$1/2^+_5$	6255	4.94(5)	6421	5.00	6490	5.15
$3/2^+_7$	6279	3.42(3)	6317	3.38*	6509	3.31*
$3/2^+_8$	6390	4.112(33)	6383	3.99*	6375	4.98*

Experimental matches were not found for two shell-model levels between 6390 and 7050 keV: a $5/2^+$ level at a calculated excitation energy of 6702 keV and another $5/2^+$ level at 7010 keV. The highest-energy state observed in the experiment was at 7.05 MeV, so we did not look for shell-model comparisons above this point. Presumably, these levels also have dominant proton-emission branches to which we were not sensitive, and it is unlikely that they contribute in large part to the ^{30}P$(p,\gamma)^{31}$S reaction rate.

VI. CONCLUSIONS

With this study we have provided a complete scheme for allowed ^{31}Cl β-delayed γ-ray transitions up to a ^{31}S excitation energy of 6390 keV, according to a comparison to our USDE shell-model calculations. 33 new γ-ray transitions and ten new β-decay transitions were observed, including the tentative first observation of a forbidden ^{31}Cl β-decay transition. The scheme reported here reflects over an order of magnitude higher statistics acquired compared to previous ^{31}Cl β-delayed γ-decay studies, and has allowed not only for positive identification of ^{31}S levels, but the definite exclusion of several previously identified ^{31}S levels. The improved accuracy of level identification in ^{31}S should assist in efforts to assign

spins and parities based on, for example, comparisons to ^{31}P mirror states. Improved ^{31}P structure studies could help to correctly deduce the parameters of the important resonances that contribute to the ^{30}P$(p,\gamma)^{31}$S reaction rate.

The ^{30}P$(p,\gamma)^{31}$S problem remains open. In the present experiment, a ^{31}S state at 6390 keV with $J^\pi = 3/2^+$ was discovered that might be the most important resonance for this reaction [6,26] at peak nova temperatures. In order to determine its strength, measurements of its proton branching ratio and lifetime are needed. It is evident from the present work that ^{31}Cl β decay is an effective channel that can be exploited to selectively populate the $3/2^+$ state in a ^{31}S excitation energy region where the density of states is quite high and measure the proton branching ratio. It is possible [26,57] that a number of negative-parity resonances contribute strongly to the reaction rate at peak nova temperatures. While the population of these negative-parity states is forbidden by the ^{31}Cl β decay selection rules, they may be accessed by other means and, if the observation of forbidden decay here is any indication, potentially even by β decay, when coupled with advanced background-reduction and coincidence techniques, using higher-intensity ^{31}Cl beams at next-generation rare isotope facilities, which hold the potential to generate orders of magnitude more statistics.

ACKNOWLEDGMENTS

We gratefully acknowledge the dedicated effort of the NSCL operations staff to ensure the delivery of multiple very pure beams. This work was supported by the US National Science Foundation under Grants No. PHY-1102511, No. PHY-1404442, No. PHY-1419765, and JINA Grant No. PHY-1430152; by the US Department of Energy, National Nuclear Security Administration under Grant No. DE-NA0000979; by the US Department of Energy, Office of Science, under Grant No. DE-SC0016052; and by the Natural Sciences and Engineering Research Council of Canada. We also gratefully acknowledge use of the Cloversharе array.

[1] L. N. Downen, C. Iliadis, J. José, and S. Starrfield, Astrophys. J. **762**, 105 (2013).
[2] E. Zinner, in *Treatise on Geochemistry, Vol. 1* (Elsevier, Amsterdam, 2003), p. 17.
[3] J. José, M. Hernanz, S. Amari, K. Lodders, and E. Zinner, Astrophys. J. **612**, 414 (2004).
[4] E. Zinner, Annu. Rev. Earth Planet Sci. **26**, 147 (1998).
[5] A. M. Davis, Proc. Natl. Acad. Sci. USA **108**, 19142 (2011).
[6] M. B. Bennett, C. Wrede, B. A. Brown, S. N. Liddick, D. Pérez-Loureiro, D. W. Bardayan, A. A. Chen, K. A. Chipps, C. Fry, B. E. Glassman, C. Langer, N. R. Larson, E. I. McNeice, Z. Meisel, W. Ong, P. D. O'Malley, S. D. Pain, C. J. Prokop, H. Schatz, S. B. Schwartz, S. Suchyta, P. Thompson, M. Walters, and X. Xu, Phys. Rev. Lett. **116**, 102502 (2016).
[7] M. Wang, G. Audi, F. G. Kondev, W. J. Huang, S. Naimi, and X. Xu, Chin. Phys. C **41**, 030003 (2017).
[8] B. A. Brown and W. A. Richter, Phys. Rev. C **74**, 034315 (2006).
[9] J. Vernotte, G. Berrier-Ronsin, S. Fortier, E. Hourani, A. Khendriche, J. M. Maison, L.-H. Rosier, G. Rotbard, E. Caurier, and F. Nowacki, Nucl. Phys. A **655**, 415 (1999).
[10] Z. Ma, D. W. Bardayan, J. C. Blackmon, R. P. Fitzgerald, M. W. Guidry, W. R. Hix, K. L. Jones, R. L. Kozub, R. J. Livesay, M. S. Smith *et al.*, Phys. Rev. C **76**, 015803 (2007).
[11] D. Irvine, A. A. Chen, A. Parikh, K. Setoodehnia, T. Faestermann, R. Hertenberger, H.-F. Wirth, V. Bildstein, S. Bishop, J. A. Clark *et al.*, Phys. Rev. C **88**, 055803 (2013).
[12] A. Kankainen, T. Eronen, S. P. Fox, H. O. U. Fynbo, U. Hager, J. Hakala, J. Huikari, D. G. Jenkins, A. Jokinen, S. Kopecky *et al.*, Eur. Phys. J. A **27**, 67 (2006).
[13] A. Saastamoinen, Studies of $T_z = -3/2$ Nuclei of Astrophysical Interest, Ph.D. thesis, University of Jyväskylä, 2011 (unpublished).
[14] D. G. Jenkins, C. J. Lister, M. P. Carpenter, P. Chowdhury, N. J. Hammond, R. V. F. Janssens, T. L. Khoo, T. Lauritsen, D. Seweryniak, T. Davinson *et al.*, Phys. Rev. C **72**, 031303(R) (2005).
[15] D. G. Jenkins, A. Meadowcroft, C. J. Lister, M. P. Carpenter, P. Chowdhury, N. J. Hammond, R. V. F. Janssens, T. L. Khoo, T. Lauritsen, D. Seweryniak *et al.*, Phys. Rev. C **73**, 065802 (2006).
[16] C. Wrede, J. A. Caggiano, J. A. Clark, C. Deibel, A. Parikh, and P. D. Parker, Phys. Rev. C **76**, 052802(R) (2007).
[17] A. Parikh, K. Wimmer, T. Faestermann, R. Hertenberger, J. José, R. Longland, H.-F. Wirth, V. Bildstein, S. Bishop, A. A. Chen *et al.*, Phys. Rev. C **83**, 045806 (2011).
[18] F. Della Vedova, Isospin Symmetry in the *sd* Shell: The $A = 31$ and $A = 35$ Mirror Nuclei, Ph.D. thesis, Universita Degli Studi di Padova, 2004 (unpublished).
[19] F. Della Vedova, S. M. Lenzi, M. Ionescu-Bujor, N. Mărginean, M. Axiotis, D. Bazzacco, A. M. Bizzeti-Sona, P. Bizzeti, A. Bracco, F. Brandolini *et al.*, Phys. Rev. C **75**, 034317 (2007).
[20] D. T. Doherty, G. Lotay, P. J. Woods, D. Seweryniak, M. P. Carpenter, C. J. Chiara, H. M. David, R. V. F. Janssens, L. Trache, and S. Zhu, Phys. Rev. Lett. **108**, 262502 (2012).
[21] D. T. Doherty, P. J. Woods, G. Lotay, D. Seweryniak, M. P. Carpenter, C. J. Chiara, H. M. David, R. V. F. Janssens, L. Trache, and S. Zhu, Phys. Rev. C **89**, 045804 (2014).
[22] C. Wrede, AIP Adv. **4**, 041004 (2014).
[23] A. Parikh, C. Wrede, and C. Fry, Eur. Phys. J. Plus **131**, 345 (2016).
[24] A. Saastamoinen, A. Kankainen, and L. Trache, Eur. Phys. J. Plus **131**, 272 (2016).
[25] M. Bouhelal and F. Haas, Eur. Phys. J. Plus **131**, 226 (2016).
[26] A. Kankainen, P. Woods, H. Schatz, T. Poxon-Pearson, D. Doherty, V. Bader, T. Baugher, D. Bazin, B. Brown, J. Browne *et al.*, Phys. Lett. B **769**, 549 (2017).
[27] C. Ouellet and B. Singh, Nucl. Data Sheets **114**, 209 (2013).
[28] M. B. Bennett, C. Wrede, K. A. Chipps, J. José, S. N. Liddick, M. Santia, A. Bowe, A. A. Chen, N. Cooper, D. Irvine *et al.*, Phys. Rev. Lett. **111**, 232503 (2013).
[29] S. B. Schwartz, C. Wrede, M. B. Bennett, S. N. Liddick, D. Pérez-Loureiro, A. Bowe, A. A. Chen, K. A. Chipps, N. Cooper, D. Irvine, E. McNeice, F. Montes, F. Naqvi, R. Ortez, S. D. Pain,

J. Pereira, C. Prokop, J. Quaglia, S. J. Quinn, J. Sakstrup, M. Santia, S. Shanab, A. Simon, A. Spyrou, and E. Thiagalingam, Phys. Rev. C **92**, 031302 (2015).
[30] D. Pérez-Loureiro, C. Wrede, M. B. Bennett, S. N. Liddick, A. Bowe, B. A. Brown, A. A. Chen, K. A. Chipps, N. Cooper, D. Irvine, E. McNeice, F. Montes, F. Naqvi, R. Ortez, S. D. Pain, J. Pereira, C. J. Prokop, J. Quaglia, S. J. Quinn, J. Sakstrup, M. Santia, S. B. Schwartz, S. Shanab, A. Simon, A. Spyrou, and E. Thiagalingam, Phys. Rev. C **93**, 064320 (2016).
[31] B. E. Glassman, D. Pérez-Loureiro, C. Wrede, J. Allen, D. W. Bardayan, M. B. Bennett, B. A. Brown, K. A. Chipps, M. Febbraro, C. Fry *et al.*, Phys. Rev. C **92**, 042501 (2015).
[32] M. B. Bennett, C. Wrede, B. A. Brown, S. N. Liddick, D. Pérez-Loureiro, D. W. Bardayan, A. A. Chen, K. A. Chipps, C. Fry, B. E. Glassman, C. Langer, N. R. Larson, E. I. McNeice, Z. Meisel, W. Ong, P. D. O'Malley, S. D. Pain, C. J. Prokop, S. B. Schwartz, S. Suchyta, P. Thompson, M. Walters, and X. Xu, Phys. Rev. C **93**, 064310 (2016).
[33] C. Wrede, B. E. Glassman, D. Pérez-Loureiro, J. M. Allen, D. W. Bardayan, M. B. Bennett, B. A. Brown, K. A. Chipps, M. Febbraro, C. Fry, M. R. Hall, O. Hall, S. N. Liddick, P. O'Malley, W.-J. Ong, S. D. Pain, S. B. Schwartz, P. Shidling, H. Sims, P. Thompson, and H. Zhang, Phys. Rev. C **96**, 032801(R) (2017).
[34] B. Glassman, D. Pérez-Loureiro, C. Wrede, J. Allen, D. Bardayan, M. Bennett, B. Brown, K. Chipps, M. Febbraro, M. Friedman, C. Fry, M. Hall, O. Hall, S. Liddick, P. O'Malley, W. Ong, S. Pain, C. Prokop, S. Schwartz, P. Shidling, H. Sims, P. Thompson, and H. Zhang, Phys. Lett. B **778**, 397 (2018).
[35] D. J. Morrissey, B. M. Sherrill, M. Steiner, A. Stolz, and I. Wiedenhoever, Nucl. Instrum. Methods Phys. Res., Sect. B **204**, 90 (2003).
[36] E. Aboud, M. B. Bennett, C. Wrede, M. Friedman, S. N. Liddick, D. Pérez-Loureiro, D. W. Bardayan, B. A. Brown, A. A. Chen, K. A. Chipps, C. Fry, B. E. Glassman, C. Langer, E. I. McNeice, Z. Meisel, W.-J. Ong, P. D. O'Malley, S. D. Pain, C. J. Prokop, H. Schatz, S. B. Schwartz, S. Suchyta, P. Thompson, M. Walters, and X. Xu (unpublished).
[37] D. Bazin, V. Andreev, A. Becerril, M. Doléans, P. F. Mantica, J. Ottarson, H. Schatz, J. B. Stoker, and J. Vincent, Nucl. Instrum. Methods Phys. Res., Sect. A **606**, 314 (2009).
[38] C. J. Prokop, S. N. Liddick, B. L. Abromeit, A. T. Chemey, N. R. Larson, S. Suchyta, and J. R. Tompkins, Nucl. Instrum. Methods Phys. Res., Sect. A **741**, 163 (2014).
[39] D. Melconian, S. Triambak, C. Bordeanu, A. Garcia, J. C. Hardy, V. E. Iacob, N. Nica, H. I. Park, G. Tabacaru, L. Trache *et al.*, Phys. Rev. C **85**, 025501 (2012).
[40] G. F. Knoll, in *Radiation Detection and Measurement*, edited by J. Welter, D. Matteson, E. S. Chew, T. Kulesa, and L. Sapira (John Wiley & Sons, New York, 2010).
[41] M. M. Be, B. Duchemin, J. Lame, C. Morillon, F. Piton, E. Browne, V. Chechev, R. Helmer, and E. Schonfeld, Table of Radionuclides, BNM-LNHB Technical Report No. CEA-ISBN 2-7272-0200-8, 1999 (unpublished).
[42] C. Ouellet and B. Singh, Nucl. Data Sheets **112**, 2199 (2011).
[43] L. Varnell and J. Trischuk, Nucl. Instrum. Methods **76**, 109 (1969).
[44] D. Wilkinson and B. Macefield, Nucl. Phys. A **232**, 58 (1974).
[45] B. A. Brown, *Lecture Notes in Nuclear Structure* (NSCL, East Lansing, MI, 2004).
[46] M. B. Bennett, Isospin Mixing and the ^{30}P$(p,\gamma)^{31}$S Reaction Rate, Ph.D. thesis, Michigan State University, 2016 (unpublished).
[47] W. A. Richter, S. Mkhize, and B. A. Brown, Phys. Rev. C **78**, 064302 (2008).
[48] F. Ajzenberg-Selove and J. L. Wiza, Phys. Rev. **143**, 853 (1966).
[49] J. M. Davidson, D. A. Hutcheon, D. R. Gill, T. Taylor, D. M. Sheppard, and W. C. Olsen, Nucl. Phys. A **240**, 253 (1975).
[50] W. P. Alford, R. N. Boyd, and D. Elmore, Phys. Rev. C **26**, 789 (1982).
[51] C. Wrede, J. A. Caggiano, J. A. Clark, C. M. Deibel, A. Parikh, and P. D. Parker, Phys. Rev. C **79**, 045803 (2009).
[52] C. E. Moss, Nucl. Phys. A **145**, 423 (1970).
[53] T. S. Bhatia, W. W. Daehnick, and G. J. Wagner, Phys. Rev. C **5**, 111 (1972).
[54] F. Didierjean and G. Walter, *Distribution of $log(ft)$ values for allowed, first and second forbidden beta transitions ($10 < A \leqslant 100$)*, CERN Technical Report No. P00022752, 1994 (unpublished).
[55] J. Hardy, L. Carraz, B. Jonson, and P. Hansen, Phys. Lett. B **71**, 307 (1977).
[56] P. M. Endt, Nucl. Phys. A **633**, 1 (1998).
[57] B. A. Brown, W. A. Richter, and C. Wrede, Phys. Rev. C **89**, 062801(R) (2014).